IEEE Access
Multidisciplinary | Rapid Review | Open Access Journal

Received March 4, 2022, accepted March 20, 2022, date of publication March 23, 2022, date of current version March 29, 2022.

Digital Object Identifier 10.1109/ACCESS.2022.3161746

A Compact Six-Port Power Divider With Two Independent Out-of-Phase Dividing Operations

MAKOTO SANO, (Member, IEEE), AND KOH HASHIMOTO, (Member, IEEE)
Wireless System Laboratory, Information and Communication Platform Laboratories, Corporate Research and Development Center, Toshiba Corporation, Kawasaki, Kanagawa 212-8582, Japan

Corresponding author: Makoto Sano (makoto8.sano@toshiba.co.jp)

ABSTRACT This paper presents a compact six-port power divider with simple structure that performs two independent out-of-phase divisions. The proposed power divider consists of a uniplanar ring crossover with four transmission lines for output and two feeding lines. The S-parameter matrix of the proposed power divider is derived analytically, and it is shown that the two independent out-of-phase divisions are realized when the circumferential length of the ring is one guided wavelength λ_g whereas conventional power dividers require a $2\lambda_g$ or $2.5\lambda_g$ ring. Two power dividers configured with striplines were designed to have -10-dB impedance bandwidths of 5% and 10% with a center frequency of 2.45 GHz. The designed power dividers were fabricated and two independent out-of-phase divisions having small amplitude imbalance were verified by measurements. Because of its compactness, the proposed power divider might be applied to the feeding network of dual-feed dual-polarized array antennas with narrow element spacing.

INDEX TERMS Dual-polarized antenna, out-of-phase power divider, ring crossover, six-port network, stripline.

I. INTRODUCTION

An out-of-phase power divider is indispensable for microwave circuitry such as push-pull amplifiers [1]–[3], balanced mixers [4], [5], and dual-feed antennas excited by a differential pair of waves [1], [6]–[9]. An out-of-phase division can be realized by a Wilkinson power divider with phase shifters [10], a slot line [11], asymmetrical coplaner lines [12], a Gysel divider [13], or even a typical 180° rat-race coupler or a magic-T junction [14].

A dual-feed dual-polarized antenna is equipped with a feeding network having two out-of-phase power dividers for two orthogonal polarizations [6]–[9]. Because the two dividers are separated, the feeding network is large in terms of wavelength [6]. Although the size can be reduced by crossing transmission lines with an air bridge [8], [9], this leads to an increase in the number of substrates or the overall height of the antenna. In addition, even with the air bridge, the element spacing of the array is still as large as about one free-space wavelength λ_0 [9]. To perform wide-angle beam steering without having grating lobes, the element spacing in rectangular arrays needs to be reduced to less than $0.5\lambda_0$ [15] by adopting a more compact feeding network.

A compact feeding network might be realized by integrating two dividers into a single divider. A single power divider for dual-feed dual-polarized antennas needs to perform two independent out-of-phase dividing operations that correspond to the inputs from two separated ports, which cannot be realized by multi-way out-of-phase dividers [16]–[18], turnstile-based orthomode transducers [19], [20], six-port junctions [21], [22], or balanced-to-unbalanced power dividers [23], [24]. Up until now, few power dividers that perform two independent out-of-phase divisions have been reported [25]–[27]. The substrate integrated waveguide (SIW) power dividers [25], [26] are unsuitable for compact networks because the width of an SIW needs to be larger than half a wavelength in order to support the dominant TE_{10} mode, and a long matching section is needed. The microstrip hybrid ring [27] does not require the matching section and is smaller than [25], [26]. However, [27] is still large for array antennas with narrow element spacing because

The associate editor coordinating the review of this manuscript and approving it for publication was Xi Zhu.

the circumferential length of the ring is $2\lambda_g$, as with the power dividers with a $2.5\lambda_g$ ring [23], [24]. Furthermore, the air bridges of microstrip lines in [27] increase the overall height and the complexity in structure.

This paper presents a six-port out-of-phase power divider composed of a four-port uniplanar ring crossover [28], [29] and two feeding lines. Because the circumferential length of the ring is only λ_g, the circuit area of proposed power divider is almost quarter of that of [27]. The proposed power divider configured with striplines is designed and constructed, and two independent out-of-phase divisions are verified.

The contributions of this paper are summarized as follows.

- A compact six-port power divider with simple structure is presented. The ring in the proposed power divider is only λ_g in circumferential length whereas the conventional hybrid-ring power dividers are composed of a $2\lambda_g$ or $2.5\lambda_g$ ring. Because the proposed power divider does not have a long matching section or the air bridges of transmission lines, the overall height and structural complexity are reduced.
- The closed-form expression of the S-parameter matrix of the proposed power divider is derived, which enables fast characterization. The characteristics of the proposed power divider are validated by both electromagnetic simulation and measurement.

The remainder of this paper is organized as follows. In Section II, the S-parameter matrix of the proposed power divider is derived, and its characteristics are studied. In Section III, two design examples of the proposed power divider configured with striplines are shown. Section IV shows the experimental results of the fabricated power dividers, including comparisons with the conventional ones. The conclusion of this paper is presented in Section V.

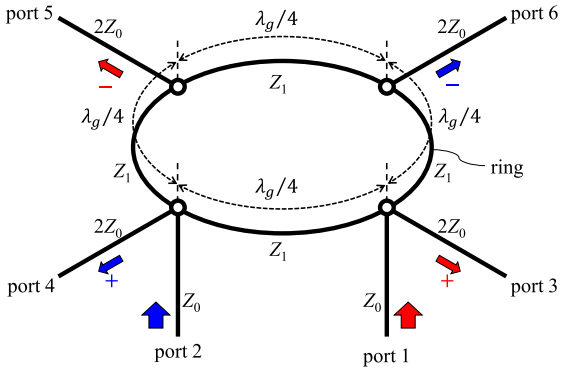

FIGURE 1. Transmission line model of the proposed six-port out-of-phase power divider that performs two independent out-of-phase divisions corresponding to the inputs from ports 1 and 2.

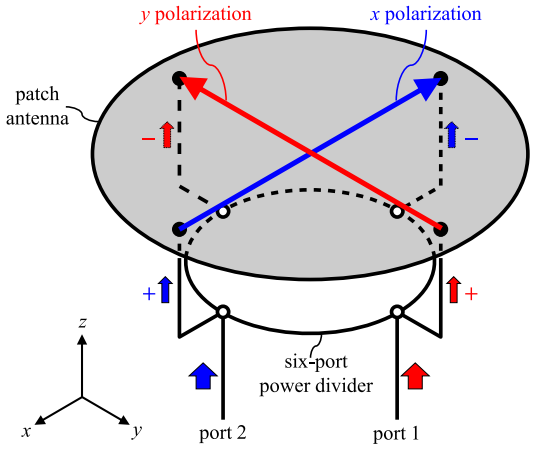

FIGURE 2. Application example: a dual-feed dual-polarized patch antenna fed by the proposed power divider.

II. ANALYSIS OF POWER DIVIDER

A. OVERVIEW

Fig. 1 shows the transmission line model of the proposed six-port out-of-phase power divider. The proposed power divider is composed of a ring crossover [28], [29] with four transmission lines for output and two feeding lines. The characteristic impedance of the four transmission lines, $2Z_0$, is twice that of the feeding lines (Z_0). The characteristic impedance of the ring is Z_1, and the circumferential length of the ring is λ_g at the center frequency f_0.

A wave input from port 1 is divided to ports 3 and 5 with opposite phases. Similarly, a wave input from port 2 is divided to ports 4 and 6 with opposite phases. The inter-port isolations, the amplitude imbalance, and so on change depending on Z_1, as will be described in Section II-C.

As an application example, a dual-feed dual-polarized patch antenna fed by the proposed power divider is shown in Fig. 2. The patch antenna is excited by a differential pair of waves, and radiates y- and x- polarized waves when ports 1 and 2 are excited, respectively. For array antennas with narrow element spacing (e.g. phased arrays with $0.5\lambda_0$ spacing), a compact feeding network is indispensable. The proposed power divider may be a promising candidate as the feeding network of these array antennas.

B. DERIVATION OF THE S-PARAMETER MATRIX

In this subsection, the S-parameter matrix of the proposed power divider is derived analytically in order to find the condition to realize two independent out-of-phase power divisions with equal-amplitude division, no reflection, and perfect inter-port isolations. Because the even–odd mode analysis [30] of a six-port network is complicated, a simple and straightforward technique based on an admittance matrix [31] was employed. To avoid several elements of the admittance matrix from diverging, nodes 1 and 2 were shifted by the phase $\Delta\psi$ as shown in Fig. 3. The limit as $\Delta\psi \to 0$ was taken after deriving the S-parameter matrix.

The element of the admittance matrix $[Y]$, $Y_{mn} = I_m/V_n|_{V_k=0\ (k\neq n)}$, is found by driving port n with voltage V_n, short-circuiting the other ports, and then calculating the current I_m at port m [14]. When nodes 1–6 on the ring shown in Fig. 3 are used as the references for ports 1–6, the admittance matrix $[Y]$ of the power divider shown in Fig. 3 is expressed as (1), shown at the bottom of the next page.

Then, the S-parameter matrix $[S]$ is obtained by

$$[S] = \left[\sqrt{\hat{Z}}\right]\left(\left[\hat{Y}\right] - [Y]\right)\left(\left[\hat{Y}\right] + [Y]\right)^{-1}\left[\frac{1}{\sqrt{\hat{Z}}}\right], \quad (2)$$

where

$$\left[\hat{Y}\right] = \mathrm{diag}\left(\frac{1}{Z_0}, \frac{1}{Z_0}, \frac{1}{Z_2}, \frac{1}{Z_2}, \frac{1}{Z_2}, \frac{1}{Z_2}, \frac{1}{Z_2}\right), \quad (3)$$

$$\left[\sqrt{\hat{Z}}\right] = \mathrm{diag}\left(\sqrt{Z_0}, \sqrt{Z_0}, \sqrt{Z_2}, \sqrt{Z_2}, \sqrt{Z_2}, \sqrt{Z_2}\right), \quad (4)$$

$$\left[\frac{1}{\sqrt{\hat{Z}}}\right] = \mathrm{diag}\left(\frac{1}{\sqrt{Z_0}}, \frac{1}{\sqrt{Z_0}}, \frac{1}{\sqrt{Z_2}}, \frac{1}{\sqrt{Z_2}}, \frac{1}{\sqrt{Z_2}}, \frac{1}{\sqrt{Z_2}}\right), \quad (5)$$

as described in [32]. By taking the limit as $\Delta\psi \to 0$, the S-parameter matrix of the power divider shown in Fig. 1 is obtained. The matrix operation in (2) and the limit operation $\Delta\psi \to 0$ were implemented with MATLAB® Symbolic Math Toolbox™ [33]. The closed-form expression of the S-parameter matrix is so long that it is not shown in this paper due to length restrictions.

When the circumferential length of the ring is λ_g (i.e. $\psi = \pi/2$), the S parameters for port 1 input are reduced to

$$S_{11} = \left(-Z_0^2Z_1^2 - 4Z_0^2Z_2^2 + Z_1^2Z_2^2 + Z_2^4\right)/\Delta_0, \quad (6)$$

$$S_{21} = -j2Z_0Z_1Z_2^2/\Delta_0, \quad (7)$$

$$S_{31} = 2\sqrt{Z_0Z_2}\left(Z_0Z_1^2 + 2Z_0Z_2^2 + Z_1^2Z_2 + Z_2^3\right)/\Delta_0, \quad (8)$$

$$S_{41} = -j2Z_0Z_1Z_2\sqrt{Z_0Z_2}/\Delta_0, \quad (9)$$

$$S_{51} = -2Z_2^2\sqrt{Z_0Z_2}\,(2Z_0 + Z_2)/\Delta_0, \quad (10)$$

$$S_{61} = -j2Z_1Z_2\sqrt{Z_0Z_2}\,(Z_0 + Z_2)/\Delta_0, \quad (11)$$

where

$$\Delta_0 = Z_0^2Z_1^2 + 4Z_0^2Z_2^2 + 2Z_0Z_1^2Z_2 + 4Z_0Z_2^3 + Z_1^2Z_2^2 + Z_2^4. \quad (12)$$

As can be derived from (8) and (10), S_{31} and S_{51} are out of phase regardless of Z_1 or Z_2. This is obvious because the difference in the path lengths from port 1 to ports 3 and 5 is $\lambda_g/2$. An equal-amplitude division ($|S_{31}| = |S_{51}|$) is realized when $Z_1 = 0$. In this case, the reflection coefficient S_{11} is further reduced to $S_{11} = (-4Z_0^2 + Z_2^2)/(4Z_0^2 + 4Z_0Z_2 + Z_2^2)$. S_{11} becomes zero when $Z_2 = 2Z_0$. The remaining elements of the S-parameter matrix are obtained by substituting $Z_1 = 0$ and $Z_2 = 2Z_0$, and finally, the S-parameter matrix of the proposed power divider for $Z_1 = 0$ is given by, (13), as shown at the bottom of the page.

Because $S_{31} = -S_{51} = 1/\sqrt{2}$, a wave input to port 1 is divided to ports 3 and 5 with opposite phases and equal amplitudes with no reflection and perfect inter-port isolations. Similarly, a wave input to port 2 is divided to ports 4 and 6 with opposite phases and equal amplitudes as $S_{42} = -S_{62}$.

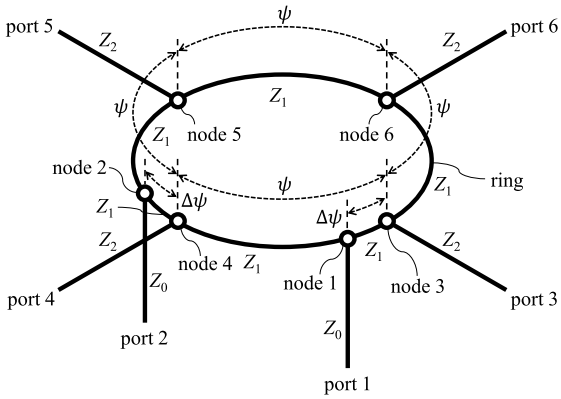

FIGURE 3. Transmission line model used for the derivation of the S-parameter matrix. ψ is the phase converted from the path length among nodes 3–6. Z_2 is the characteristic impedance of the four transmission lines for output.

C. PARAMETRIC STUDY OF THE POWER DIVIDER

In Section II-B, it was shown that two independent out-of-phase divisions are realized when the circumferential length of the ring is λ_g as in Fig. 1. It was also shown that equal-amplitude division, no reflection, and perfect inter-port isolations are realized when $Z_1 = 0$ and $Z_2 = 2Z_0$. In actual transmission lines, however, $Z_1 = 0$ cannot be realized.

$$[Y] = \frac{j}{Z_1}\begin{bmatrix} -\cot\Delta\psi - \cot(\psi - \Delta\psi) & 0 & \csc\Delta\psi & \csc(\psi - \Delta\psi) & 0 & 0 \\ 0 & -\cot\Delta\psi - \cot(\psi - \Delta\psi) & 0 & \csc\Delta\psi & \csc(\psi - \Delta\psi) & 0 \\ \csc\Delta\psi & 0 & -\cot\Delta\psi - \cot\psi & 0 & 0 & \csc\psi \\ \csc(\psi - \Delta\psi) & \csc\Delta\psi & 0 & -\cot(\psi - \Delta\psi) - \cot\Delta\psi & 0 & 0 \\ 0 & \csc(\psi - \Delta\psi) & 0 & 0 & -\cot(\psi - \Delta\psi) - \cot\psi & \csc\psi \\ 0 & 0 & \csc\psi & 0 & \csc\psi & -2\cot\psi \end{bmatrix} \quad (1)$$

$$[S] = \begin{bmatrix} 0 & 0 & 1/\sqrt{2} & 0 & -1/\sqrt{2} & 0 \\ 0 & 0 & 0 & 1/\sqrt{2} & 0 & -1/\sqrt{2} \\ 1/\sqrt{2} & 0 & -1/2 & 0 & -1/2 & 0 \\ 0 & 1/\sqrt{2} & 0 & -1/2 & 0 & -1/2 \\ -1/\sqrt{2} & 0 & -1/2 & 0 & -1/2 & 0 \\ 0 & -1/\sqrt{2} & 0 & -1/2 & 0 & -1/2 \end{bmatrix}. \quad (13)$$

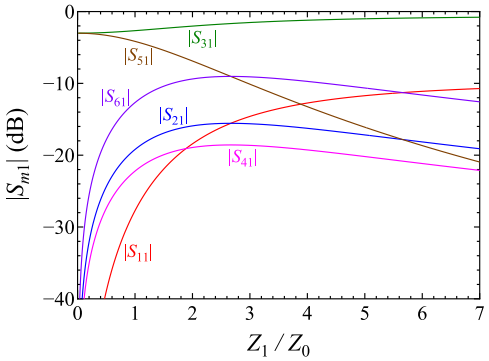

FIGURE 4. $|S_{m1}|$ ($m = 1, \ldots, 6$) of the proposed power divider at the center frequency f_0.

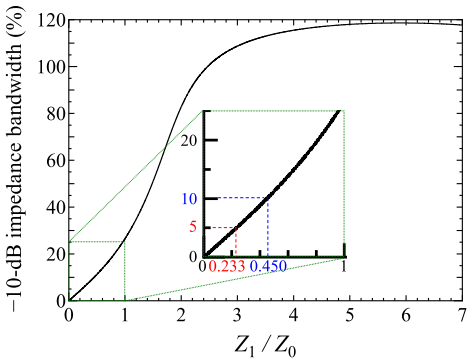

FIGURE 5. −10-dB impedance bandwidth as a function of the normalized characteristic impedance Z_1/Z_0.

To study the characteristics of the proposed power divider with a realistic value of Z_1, the S parameters were calculated by sweeping Z_1 (> 0) with Z_2 fixed to $2Z_0$. Fig. 4 shows $|S_{m1}|$ as a function of the normalized characteristic impedance Z_1/Z_0. $|S_{11}|$, $|S_{21}|$, $|S_{41}|$, and $|S_{61}|$, as well as the amplitude imbalance between $|S_{31}|$ and $|S_{51}|$ increase with Z_1/Z_0, whereas the phase difference between S_{31} and S_{51} remains constant at $-180°$ regardless of Z_1/Z_0, as explained in Section II-B. The S parameters for the port 2 input, S_{m2}, are not shown because the tendency of S_{m2} is the same as that of S_{m1} due to the symmetrical structure.

The frequency characteristics can be obtained by substituting $\psi = (\pi/2) \cdot (f/f_0)$ into (1), where f is the frequency. The −10-dB impedance bandwidth, the fractional bandwidth for the reflection $|S_{11}|$ below −10 dB, as a function of Z_1/Z_0 is shown in Fig. 5. The bandwidth increases with Z_1/Z_0, and reaches the maximum of 118.6% when $Z_1/Z_0 = 5.89$. However, the amplitude imbalance between $|S_{31}|$ and $|S_{51}|$ is as large as 20.2 dB in this case. The reflection and the inter-port isolations are also high. To reduce the amplitude imbalance, the reflection, and the inter-port isolations, smaller value of Z_1/Z_0 needs to be chosen. When $Z_1/Z_0 = 0.450$, for instance, a 10% bandwidth is obtained as shown in Fig. 5. The amplitude imbalance at f_0 is 0.32 dB in this case. When $Z_1/Z_0 = 0.233$, the amplitude imbalance at f_0 is reduced to 0.09 dB. Meanwhile, the bandwidth is also reduced to 5%.

As explained above, there is a trade-off between the impedance bandwidth and the other parameters, including the inter-port isolations and the amplitude imbalance. Based on Figs. 4 and 5, Z_1/Z_0 can be determined by considering the impedance bandwidth, amplitude imbalance, reflection, and inter-port isolations that are acceptable for the applications of the proposed power divider.

III. DESIGN OF THE POWER DIVIDER

A. CONFIGURATION

A power divider configured with striplines is shown in Fig. 6. Two 0.75-mm-thick polyphenylene ether (PPE) substrates (dielectric constant $\varepsilon_r = 3.64$ and loss tangent $\tan\delta = 0.002$) are stacked and glued with a 5-μm-thick bonding film

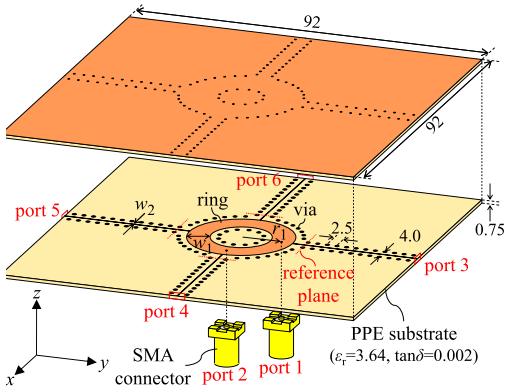

FIGURE 6. Power divider configured with striplines. A 5 μm-thick bonding film (not shown) was used to glue two PPE substrates. $r_1 = 10.50$, $w_2 = 0.14$. $w_1 = 5.78$ (5%), 2.67 (10% bandwidth). Unit: mm.

($\varepsilon_r = 2.50$ and $\tan\delta = 0.002$). To facilitate its application as the feeding network of antenna arrays, two SMA connectors are mounted on the bottom layer of the substrate. Ports 1 and 2 are assigned at the ends of the SMA connectors with $Z_0 = 50\Omega$. The reference planes of ports 3–6 are shown as red dotted lines in Fig. 6. To prevent the parallel-plate mode from traveling, metallic vias are placed along the striplines.

B. DESIGN PROCEDURES

As examples, two power dividers were designed to have 5% and 10% bandwidths at 2.45 GHz, in the following steps. Electromagnetic simulations were performed using Ansys® HFSS™ [34].

1) The width of the four striplines for output, w_2, was chosen to be 0.14 mm in order to have the characteristic impedance of 100Ω ($= 2Z_0$).
2) Based on the relation between Z_1/Z_0 and the bandwidth described in Section II-C, the widths of the ring w_1 were chosen to be 5.78 mm and 2.67 mm in order to have the characteristic impedances 11.5Ω ($= 0.233\, Z_0$) and 22.5Ω ($= 0.450\, Z_0$) for 5% and 10% bandwidths, respectively.
3) The radius of the ring r_1 was determined to minimize the reflection at 2.45 GHz. r_1 was determined based

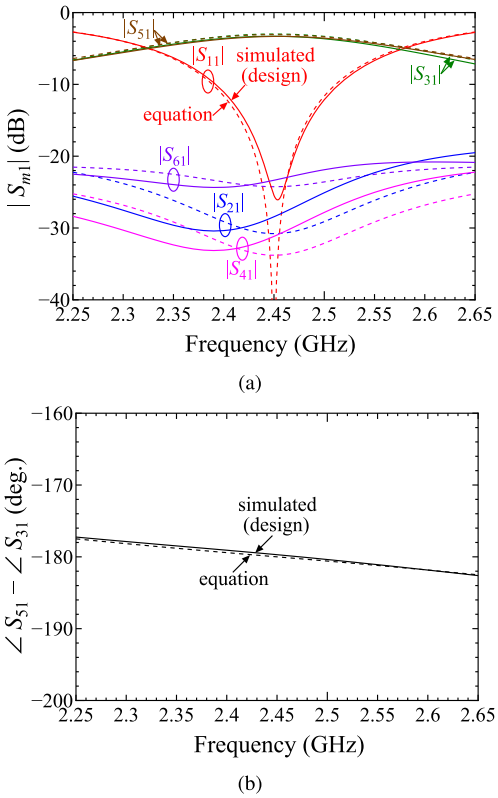

FIGURE 7. *S* parameters of the power divider designed to have 5% bandwidth. The *S* parameters obtained by equation (dotted line) and the electromagnetic simulation (solid line) are compared. (a) $|S_{m1}|(m = 1, \ldots, 6)$. (b) Phase difference between S_{31} and S_{51}.

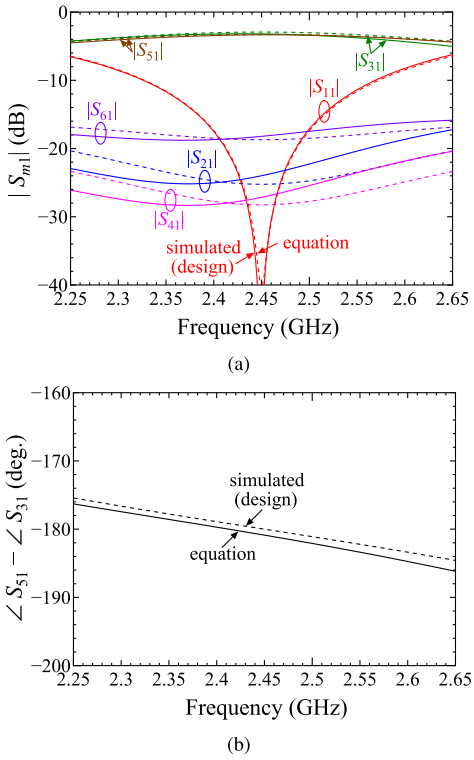

FIGURE 8. *S* parameters of the power divider designed to have 10% bandwidth. (a) $|S_{m1}|(m = 1, \ldots, 6)$. (b) Phase difference between S_{31} and S_{51}.

on the reflection (not on the circumferential length) because it is difficult to know the guided wavelength in the ring.

C. SIMULATED RESULTS

The *S* parameters of the power dividers designed to have 5% and 10% bandwidths are shown in Figs. 7 and 8, respectively. The *S* parameters obtained by the electromagnetic simulation are similar to those obtained by the equations. The −10-dB impedance bandwidths obtained by the simulation are 5.01% and 9.92%, which are in a good agreement with the desired ones (5% and 10%). The simulated amplitude imbalances of the power dividers (5% and 10% bandwidths) are 0.02 dB and 0.13 dB at 2.45 GHz, respectively. The simulated S_{31} and S_{51} are almost out of phase as shown in Figs. 7(b) and 8(b). The losses in the power dividers (5% and 10% bandwidths) are 0.26 dB and 0.16 dB, respectively. The discrepancy in the *S* parameters obtained by the equations and the simulation may come from the SMA connectors and the structural discontinuities that are not considered in the equations.

IV. MEASURED RESULTS

The power dividers designed in Section III were fabricated (Fig. 9). To show the striplines printed on the inner layer, non-laminated substrates were also fabricated in another lot.

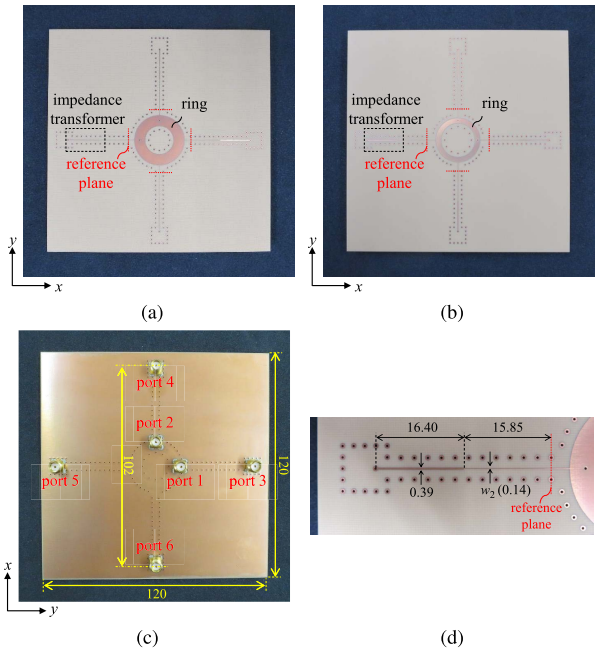

FIGURE 9. Fabricated power divider. (a) Inner layer (5% bandwidth). (b) Inner layer (10%). (c) Bottom layer (5%). (d) Quarter-wavelength impedance transformer (5%). Unit: mm.

The inner layers of the power dividers are shown in Figs. 9(a) and (b). To connect the striplines with the SMA connectors having different characteristic impedances,

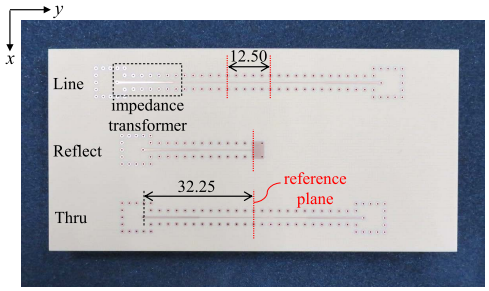

FIGURE 10. Thru, reflection, and line patterns for the TRL calibration. Unit: mm.

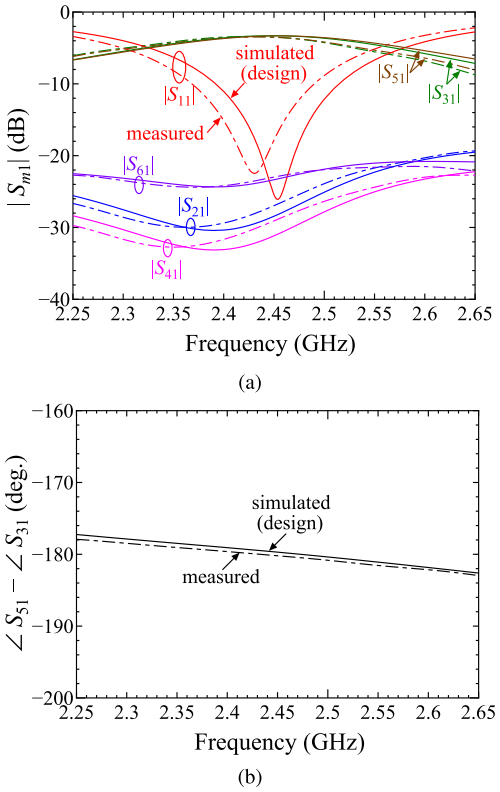

FIGURE 11. Measured (dashed–dotted line) and simulated (solid line) S parameters of the power divider designed to have a 5% bandwidth. (a) $|S_{m1}|(m = 1, \ldots, 6)$. (b) Phase difference between S_{31} and S_{51}.

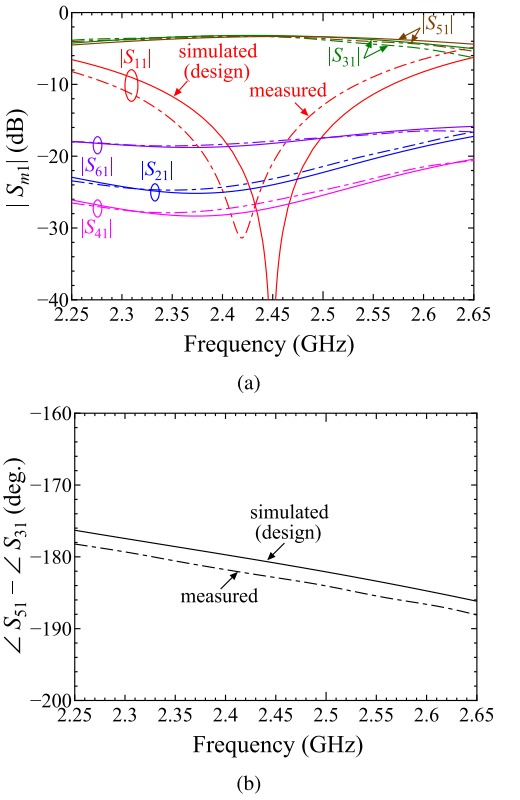

FIGURE 12. Measured (dashed–dotted line) and simulated (solid line) S parameters of the power divider designed to have a 10% bandwidth. (a) $|S_{m1}|(m = 1, \ldots, 6)$. (b) Phase difference between S_{31} and S_{51}.

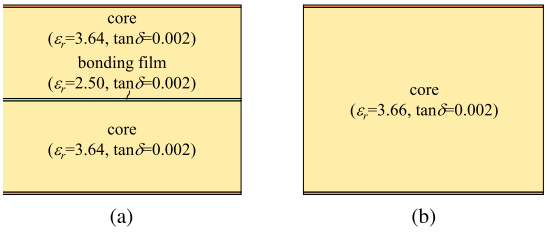

FIGURE 13. Layer configuration of the substrates. (a) Configuration used in the design. (b) Configuration for the re-simulation with the estimated effective dielectric constant ε_r.

quarter-wavelength impedance transformers were inserted between them, as shown in Fig. 9(d).

The S parameters of the fabricated power divider were measured. The effect of the SMA connectors and the impedance transformers were eliminated by the TRL (Thru-Reflect-Line) calibration [14], using the Thru, Reflect, and Line patterns shown in Fig. 10. The reference planes for ports 3–6 are shown as red dotted lines in Figs. 9(a) and (b). The measured S parameters are shown in Figs. 11 and 12. The measured S parameters have a similar tendency to the simulated ones except for a slight shift in frequency. The measured −10-dB impedance bandwidths of the power dividers are 5.01% and 10.0%, which are close to the desired ones (5% and 10%, respectively). The amplitude imbalances of the power dividers (5% and 10% bandwidths) measured at 2.45 GHz are 0.04 dB and 0.01 dB, respectively. The losses in the power dividers (5% and 10% bandwidths) measured at 2.45 GHz are 0.37 dB and 0.04 dB, respectively. The measured S_{31} and S_{51} are almost out of phase as shown in Figs. 11(b) and 12(b). Although not shown in this paper, similar tendencies of the measured S parameters for the port 2 input, S_{m2}, were also observed. Given that $S_{31} \simeq -S_{51}$ and $S_{42} \simeq -S_{62}$, two independent out-of-phase divisions with a small amplitude imbalance have been verified by measurements.

A shift in the frequency is often caused by the difference between the dielectric constant of substrates considered in the design process and that of the actual substrates. The actual dielectric constant may differ from that on the datasheet as

TABLE 1. Comparison of six-port power dividers having two input ports.

Reference	Geometry	Transmission line	Center frequency f_0	Circuit area [a] $\lambda_0 \times \lambda_0$ $(\lambda_g \times \lambda_g)$	−10-dB impedance bandwidth	Out-of-phase division	Two independent divisions
[21]	T junctions and hybrid couplers	SIW	24 GHz	$3.5\lambda_0 \times 5.3\lambda_0$ $(3.5\lambda_g \times 5.4\lambda_g)$	N/A	No	No
[22]	T junctions and hybrid couplers	ridge-gap waveguide	40 GHz	$5.1\lambda_0 \times 5.1\lambda_0$ (N/A)	N/A	No	No
[23]	$2.5\lambda_g$ ring	microstrip line	2.0 GHz	$0.52\lambda_0 \times 0.34\lambda_0$ $(0.77\lambda_g \times 0.50\lambda_g)$	46%	Yes	No
[24] (rat-race type 1)	$2.5\lambda_g$ ring	microstrip line	1.02 GHz	$0.21\lambda_0 \times 0.33\lambda_0$ $(0.34\lambda_g \times 0.52\lambda_g)$	17%	Yes	No
[24] (rat-race type 2)	$2.5\lambda_g$ ring	microstrip line	1.01 GHz	$0.22\lambda_0 \times 0.27\lambda_0$ $(0.34\lambda_g \times 0.43\lambda_g)$	31%	Yes	No
[25]	cross junction with a coupling slot	SIW	60 GHz	$1.4\lambda_0 \times 1.4\lambda_0$ $(1.6\lambda_g \times 1.6\lambda_g)$	>33% [b]	Yes	Yes
[26]	cross junction with a coupling slot	SIW	20 GHz	$0.84\lambda_0 \times 0.84\lambda_0$ $(1.2\lambda_g \times 1.2\lambda_g)$	15% [b]	Yes	Yes
[27]	$2\lambda_g$ ring with air bridges	microstrip line	2.3 GHz	$0.44\lambda_0 \times 0.44\lambda_0$ $(0.67\lambda_g \times 0.67\lambda_g)$	>65% [b]	Yes	Yes
This work (5% bandwidth)	λ_g ring	stripline	2.43 GHz	$0.22\lambda_0 \times 0.22\lambda_0$ $(0.40\lambda_g \times 0.40\lambda_g)$	5.01%	Yes	Yes
This work (10% bandwidth)	λ_g ring	stripline	2.42 GHz	$0.19\lambda_0 \times 0.19\lambda_0$ $(0.36\lambda_g \times 0.36\lambda_g)$	10.0%	Yes	Yes

[a] rectangular area encompassing a divider. λ_0 and λ_g are free-space and guided wavelengths at f_0, respectively. [b] Simulated value.

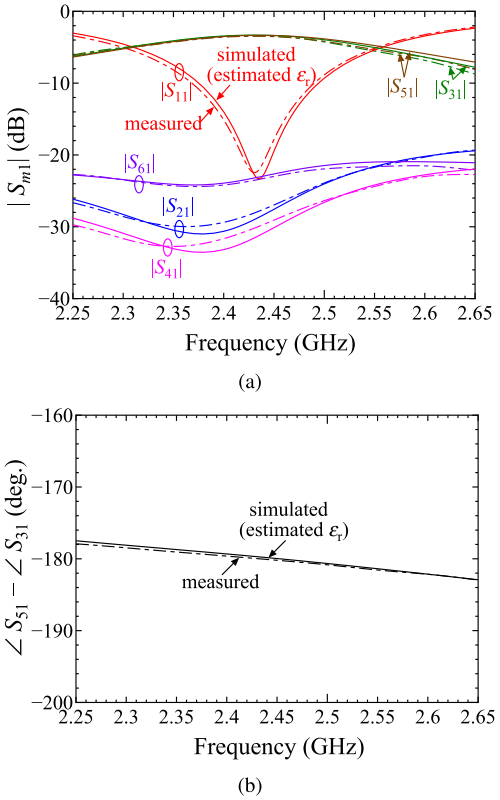

FIGURE 14. *S* parameters of the power divider having a 5% bandwidth. Measured (dashed–dotted line) and simulated with the estimated effective dielectric constant ε_r (solid line) are compared. (a) $|S_{m1}|(m = 1, \ldots, 6)$. (b) Phase difference between S_{31} and S_{51}.

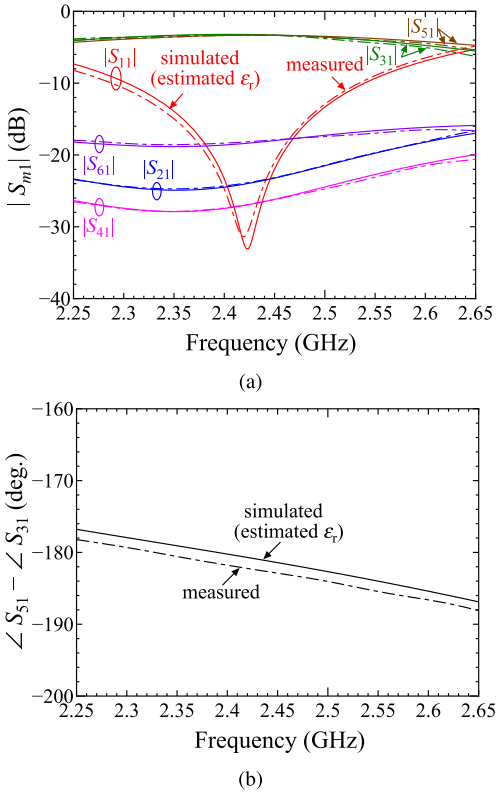

FIGURE 15. *S* parameters of the power divider having a 10% bandwidth. (a) $|S_{m1}|(m = 1, \ldots, 6)$. (b) Phase difference between S_{31} and S_{51}.

explained in [35]. To estimate the effective dielectric constant of the fabricated substrates, the Line-Line (LL) method [36] was applied to the measured results of the Thru and Line patterns shown in Fig. 10. The effective dielectric constant ε_r, including the effect of the bonding film, was found to be 3.66 at 2.45 GHz. The layer configuration of the substrates was modified for re-simulation as shown in Fig. 13. The value of tan δ was kept to 0.002 because the estimated tan δ

(0.014 at 2.45 GHz) includes the effects of both the dielectric and conductor losses that are difficult to decompose. Figs. 14 and 15 show the S parameters measured and simulated with the estimated ε_r. The frequency shift is mitigated by using the estimated ε_r. The error in the phase is still observed in Fig. 15(b), which might come from the solder and the misalignment of the SMA connectors that were not considered in the re-simulation.

Six-port power dividers having two input ports are compared in Table 1. The six-port junctions [21], [22] are large in terms of wavelength because they are composed of multiple dividers and couplers. Furthermore, additional baluns are needed in order to perform out-of-phase division, which leads to even larger size. Although smaller size and out-of-phase division without additional baluns are realized with hybrid rings [23], [24], they cannot perform two independent divisions required for dual-feed dual-polarized antennas. The SIW power dividers [25], [26] can perform two independent out-of-phase divisions. However, the matching section increases overall circuit size. The air bridges in [27] increase the number of substrates and structural complexity as well. Whereas the conventional hybrid rings are $2\lambda_g$ [27] or $2.5\lambda_g$ [23], [24] in circumferential length, the proposed ones are based on a λ_g ring without air bridges or matching sections. Because of the compact ring, the circuit area of the proposed power divider is about quarter of that of [27]. Although the bandwidths of the presented power dividers (5% and 10%) are relatively narrow, the bandwidth can be enhanced by choosing larger Z_1/Z_0 as described in II-C. Because of the compactness, the proposed power divider could be integrated in the feeding network of array antenna with narrow element spacing.

V. CONCLUSION

This paper presented a compact six-port power divider with simple structure that performs two independent out-of-phase divisions. The S-parameter matrix of the proposed power divider was derived analytically, and it was shown that two independent out-of-phase divisions are realized with a λ_g ring, whereas the conventional hybrid-ring power dividers are based on a $2\lambda_g$ or $2.5\lambda_g$ ring. In addition, the proposed power divider does not require the air bridges of transmission lines [27] that increase overall size and structural complexity, which could lead to low-cost and stable fabrication.

Two power dividers configured with striplines were designed to have -10-dB impedance bandwidths of 5% and 10% with a center frequency of 2.45 GHz. The designed power dividers were fabricated and measured, and two independent out-of-phase divisions with small amplitude imbalance were verified. The shift in the frequency was explained by the difference in the effective dielectric constants.

Whereas the proposed power divider has a narrower bandwidth compared with the conventional ones, the proposed power divider is much smaller in terms of wavelength. Because of its compactness, the proposed power divider could be adopted to the feeding network of dual-feed dual-polarized antenna arrays with narrow element spacing. Design of dual-feed dual-polarized antenna arrays equipped with the proposed power divider is a future research topic.

REFERENCES

[1] W. R. Deal, V. Radisic, Y. Qian, and T. Itoh, "Integrated-antenna push-pull power amplifiers," *IEEE Trans. Microw. Theory Techn.*, vol. 47, no. 8, pp. 1418–1425, Aug. 1999.

[2] L. Chiu, T. Y. Yum, Q. Xue, and C. H. Chan, "A wideband compact parallel-strip 180° Wilkinson power divider for push-pull circuitries," *IEEE Microw. Wireless Compon. Lett.*, vol. 16, no. 1, pp. 49–51, Jan. 2006.

[3] W. Feng, Y. Shi, X. Y. Zhou, X. Shen, and W. Che, "A bandpass push–pull high power amplifier based on SIW filtering balun power divider," *IEEE Trans. Plasma Sci.*, vol. 47, no. 9, pp. 4281–4286, Sep. 2019.

[4] K. Yhland, N. Rorsman, and H. H. G. Zirath, "Novel single device balanced resistive HEMT mixers," *IEEE Trans. Microw. Theory Techn.*, vol. 43, no. 12, pp. 2863–2867, Dec. 1995.

[5] Y. Lin, J. Lee, S. Huang, C. Wang, C. Wang, and S. Lu, "Design and analysis of a 21–29-GHz ultra-wideband receiver front-end in 0.18-μm CMOS technology," *IEEE Trans. Microw. Theory Techn.*, vol. 60, no. 8, pp. 2590–2604, Aug. 2012.

[6] K. S. Ryu and A. A. Kishk, "Wideband dual-polarized microstrip patch excited by hook shaped probes," *IEEE Trans. Antennas Propag.*, vol. 56, no. 12, pp. 3645–3649, Dec. 2008.

[7] K. L. Wong, H. C. Tung, and T. W. Chiou, "Broadband dual-polarized aperture-coupled patch antennas with modified H-shaped coupling slots," *IEEE Trans. Antennas Propag.*, vol. 50, no. 2, pp. 188–191, Feb. 2002.

[8] Z. Tang, J. Liu, R. Lian, Y. Li, and Y. Yin, "Wideband differentially fed dual-polarized planar antenna and its array with high common-mode suppression," *IEEE Trans. Antennas Propag.*, vol. 67, no. 1, pp. 131–139, Jan. 2019.

[9] J. Zhang, X. Q. Lin, L. Y. Nie, J. W. Yu, and Y. Fan, "Wideband dual-polarization patch antenna array with parallel strip line balun feeding," *IEEE Antennas Wireless Propag. Lett.*, vol. 15, pp. 1499–1501, 2016.

[10] M. A. Antoniades and G. V. Eleftheriades, "A broadband Wilkinson balun using microstrip metamaterial lines," *IEEE Antennas Wireless Propag. Lett.*, vol. 4, pp. 209–212, 2005.

[11] M. E. Bialkowski and A. M. Abbosh, "Design of a compact UWB out-of-phase power divider," *IEEE Microw. Wireless Compon. Lett.*, vol. 17, no. 4, pp. 289–291, Apr. 2007.

[12] L. Fan and K. Chang, "A 180° out-of-phase power divider using asymmetrical coplanar stripline," *IEEE Microw. Guided Wave Lett.*, vol. 6, no. 11, pp. 404–406, Nov. 1996.

[13] A. M. Abbosh, "Planar out-of-phase power divider/combiner for wideband high power microwave applications," *IEEE Trans. Compon., Packag., Manuf. Technol.*, vol. 4, no. 3, pp. 465–471, Mar. 2014.

[14] D. M. Pozar, *Microwave Engineering*, 4th ed. New York, NY, USA: Wiley, 2011.

[15] R. J. Mailloux, *Phased Array Handbook*, 3rd ed. Norwood, MA, USA: Artech House, 2018.

[16] T. Yang, J. X. Chen, and Q. Xue, "Three-way out-of-phase power divider," *Electron. Lett.*, vol. 44, no. 7, pp. 482–483, Mar. 2008.

[17] K. Song, Y. Mo, Q. Xue, and Y. Fan, "Wideband four-way out-of-phase slotline power dividers," *IEEE Trans. Ind. Electron.*, vol. 61, no. 7, pp. 3598–3606, Jul. 2014.

[18] C.-G. Sun, J.-L. Li, and B. A. Twumasi, "Multi-way differential power divider with microstrip output interfaces," *J. Electr. Eng.*, vol. 71, no. 4, pp. 274–280, Sep. 2020.

[19] M. A. Meyer and H. B. Goldberg, "Applications of the turnstile junction," *IRE Trans. Microw. Theory Techn.*, vol. 3, no. 6, pp. 40–45, Dec. 1955.

[20] A. Navarrini and R. L. Plambeck, "A turnstile junction waveguide orthomode transducer," *IEEE Trans. Microw. Theory Techn.*, vol. 54, no. 1, pp. 272–277, Jan. 2006.

[21] X. Xu, R. G. Bosisio, and K. Wu, "A new six-port junction based on substrate integrated waveguide technology," *IEEE Trans. Microw. Theory Techn.*, vol. 53, no. 7, pp. 2267–2273, Jul. 2005.

[22] X. Jiang, Y. Shi, F. Jia, W. Feng, T. Yin, J. Yu, and X. Wang, "Millimeter-wave double ridge gap waveguide six-port network based on multi-via mushroom," *IEEE Trans. Plasma Sci.*, vol. 49, no. 12, pp. 3778–3785, Dec. 2021.

[23] L. Li, L. S. Wu, and J.-F. Mao, "A balanced-to-unbalanced hybrid ring with arbitrary power division ratio," *IEEE Access*, vol. 6, pp. 19784–19790, 2018.
[24] L. Jiao, Y. Wu, W. Zhang, M. Li, Y. Liu, Q. Xue, and Z. Ghassemlooy, "Design methodology for six-port equal/unequal quadrature and rat-race couplers with balanced and unbalanced ports terminated by arbitrary resistances," *IEEE Trans. Microw. Theory Techn.*, vol. 66, no. 3, pp. 1249–1262, Mar. 2018.
[25] Y. Zhao and K.-M. Luk, "Dual circular-polarized SIW-fed high-gain scalable antenna array for 60 GHz applications," *IEEE Trans. Antennas Propag.*, vol. 66, no. 3, pp. 1288–1298, Mar. 2018.
[26] Q. Yang, S. Gao, Q. Luo, L. Wen, X. Ren, J. Wu, Y.-L. Ban, and X.-X. Yang, "A dual-polarized planar antenna array differentially-fed by orthomode transducer," *IEEE Trans. Antennas Propag.*, vol. 69, no. 5, pp. 2637–2647, May 2021.
[27] X.-J. Lin, Z.-M. Xie, and P.-S. Zhang, "High isolation dual-polarized patch antenna with hybrid ring feeding," *Int. J. Antennas Propag.*, vol. 2017, pp. 1–6, May 2017.
[28] F. Tefiku and E. Yamashita, "Improved analysis method for multiport microstrip annular-ring power-dividers," *IEEE Trans. Microw. Theory Techn.*, vol. 42, no. 3, pp. 376–382, Mar. 1994.
[29] Y. Chen and S.-P. Yeo, "A symmetrical four-port microstrip coupler for crossover application," *IEEE Trans. Microw. Theory Techn.*, vol. 55, no. 11, pp. 2434–2438, Nov. 2007.
[30] J. Reed and G. J. Wheeler, "A method of analysis of symmetrical four-port networks," *IRE Trans. Microw. Theory Techn.*, vol. 4, no. 4, pp. 1244–1245, Oct. 1956.
[31] C. Miao, G. Tian, J. Yang, and W. Wu, "Analysis of multiport passive components using admittance matrix," in *Proc. Int. Conf. Microw. Millim. Wave Technol. (ICMMT)*, May 2012, pp. 1–4.
[32] R. Mavaddat, *Network Scattering Parameters*. Singapore: World Scientific, 1996.
[33] MathWorks. *MATLAB Symbolic Math Toolbox™*. Accessed: Mar. 23, 2022. [Online]. Available: https://www.mathworks.com/help/symbolic/
[34] Ansys. *HFSS™*. Accessed: Mar. 23, 2022. [Online]. Available: https://www.ansys.com/products/electronics/ansys-hfss
[35] IPC. *IPC-TM-650 Test Methods Manual*. Accessed: Mar. 23, 2022. [Online]. Available: https://www.ipc.org/sites/default/files/test_methods_docs/2-5_2-5-5-5-1.pdf
[36] I. Huynen, C. Steukers, and F. Duhamel, "A wideband line-line dielectrometric method for liquids, soils, and planar substrates," *IEEE Trans. Instrum. Meas.*, vol. 50, no. 5, pp. 1343–1348, Oct. 2001.

MAKOTO SANO (Member, IEEE) was born in Shizuoka, Japan, in November 1987. He received the B.S., M.S., and D.E. degrees in electrical and electronic engineering from the Tokyo Institute of Technology, Tokyo, Japan, in 2010, 2012, and 2015, respectively. During his doctoral studies, he spent three months with the Technical University of Madrid, Madrid, Spain. Since 2015, he has been working at Toshiba Corporation. His research interests include array antennas and near-field antenna measurement. He received the IEEE AP-S Tokyo Chapter Young Engineer Award, in 2020. He is also a member of the Institute of Electronics, Information and Communication Engineers (IEICE). He has been an Associate Editor of *IEICE Electronics Express*, since 2018.

KOH HASHIMOTO (Member, IEEE) was born in Tokyo, Japan, in January 1982. He received the B.S., M.S., and D.E. degrees in electrical and electronic engineering from the Tokyo Institute of Technology, Tokyo, in 2005, 2007, and 2010, respectively. He joined the Research and Development Center, Toshiba Corporation, Kawasaki, Japan, in 2010. His research interests include array antennas and millimeter-wave antennas. He is a member of the Institute of Electrical, Information and Communication Engineers (IEICE), Japan.